Journal of Materials Chemistry A

Accepted Manuscript

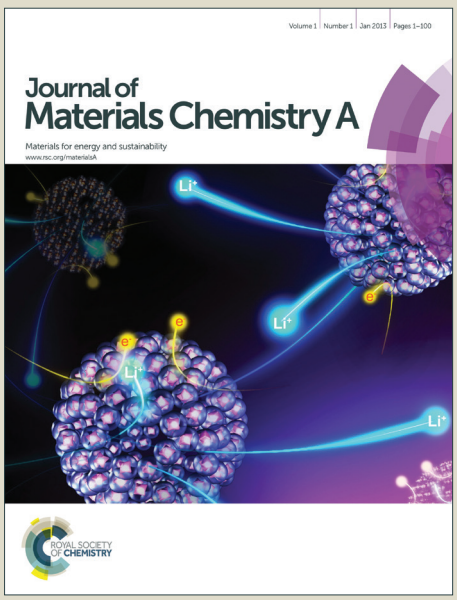

ROYAL SOCIETY OF CHEMISTRY

www.rsc.org/materialsA

Cite this: DOI: 10.1039/c0xx00000x

www.rsc.org/xxxxxx

Paper

Layered polyaniline/graphene film from sandwich-structured polyaniline/graphene/polyaniline nanosheets for high-performance pseudosupercapacitors

Zhongqiu Tong[a], Yongning Yang[a], Jiayu Wang[a], Jiupeng Zhao*[b], Bao-Lian Su[c] and Yao Li*[a]

Received (in XXX, XXX) Xth XXXXXXXXX 20XX, Accepted Xth XXXXXXXXX 20XX
DOI: 10.1039/b000000x

Binder-free layered graphene/polyaniline composite film was prepared by an environmental-friendly and facile two-step route for the first time. Firstly, sandwich-structured PANI/graphene/PANI nanosheet was in situ prepared from aqueous solution, followed an electrophoretic deposition process. By observations of scanning electron microscopy (SEM), transmission electron microscopy (TEM) and atomic force microscopy (AFM), it conforms that the graphene sheet is uniformly covered by an ultrathin PANI film (3.7 nm). Raman spectra, Fourier transform infrared (FT-IR) spectra and X-Ray photoelectron spectroscopy (XPS) are jointly used to confirm strong π-π electron and hydrogen bond interaction in the nanosheets. The layered PANI/graphene composite film exhibits an excellent gravimetric capacitance of 384 F g^{-1} at 0.5 A g^{-1} which is much higher than many other hybrid supercapacitor reported to date. It maintains its capacity up to 84% over 1000 cycles at a current density of 2 A g^{-1}. This preparation method may provide a promising strategy for preparation of graphene-based composites with other conducting polymers and binder-free film electrodes.

Introduction

Nowadays, with the increasing use of portable electronic devices, electric vehicles and other electronic products, electrical energy storage becomes more important than any time in the past [1]. Among various energy storage methods, supercapacitor is a promising kind of energy storage system [2]. According to their energy-storage mechanism, supercapacitors can be basically classified into electrical double-layer capacitors (EDLCs) and pseudocapacitors [3]. In carbon-based EDLCs, the capacitance arises from surface charge accumulation as a result of rapid adsorption/desorption of electrolyte ions at the electrode/electrolyte interface, thereby leading to fast response and long cycle life but relatively low specific capacitance [4,5]. On the other hand, pseudocapacitors exhibit higher energy storage capacity because of faradic electron-transfer processes of electroactive metal oxides and conducting polymers [6,7]. However, they suffered poor stabilities during charge/discharge processes.

Polyaniline (PANI) is a well-studied conducting polymer for pseudocapacitors due to its ease of synthesis, environmental stability and the high specific capacitance from multiple doping/dedoping states [8]. However, when used as bulk materials, during the charge/discharge circles, the repeating counter ions insertation/deinsertation process caused serious volume change, which made PANI exhibit a limited stability [9,10]. Composites of PANI and carbon have been reported as promising prototype materials for supercapacitor applications [11]. Graphene, emerging as a new two-dimensional material with atomic thickness, has now aroused tremendous attention worldwide due to several breakthroughs in fundamental research and promising practical applications [12-14]. Additionally, graphite oxide (GO) with active oxygen functionalities on their planes facilitate surface modification for making composites with other materials, such as conducting polymers [15]. The excellent properties of graphene and the advantages of PANI have attracted great research interests in preparing graphene/PANI composites for pseudosupercapacitors [15-26]. Further, because of the PANI's intrinsic semiconductor properties and enhanced electrical conductivity in the graphene/PANI composites, these composites also showed wide applications in thermoelectricity [27,28], solar cells [29,30] and semiconductor devices [31]. Much promising research has been reported to date on preparation graphene/PANI composites, including *in situ* chemical oxidation polymerization [18-22], electropolymerization [7,16] and electrostatic adsorption assembly [23-26]. Electrodes based on graphene/PANI powders have usually been achieved by using a binder (usually polyfluortetraethylene or polyvinylidene fluoride) to stick the active composite materials onto collector electrodes [18-22]. Mixture of an insulating binder not only makes the preparation procedures more complex, but also reduces the electrochemical active surface area and wastes energy on unwanted inner resistance [23]. Further, due to a lack of precise control over the nano-architechture, these composites showed poor utilization of the graphene's intrinsic high surface and intimate electrochemical interfaces between PANI and graphene [25]. Therefore, it continues to be a challenging endeavor to prepare nanoscale uniform blend graphene/PANI composites with intimate electrochemical interfaces.

In this paper, the sandwich-structured PANI/graphene/PANI nanosheets with ultrathin PANI film (3.7 nm) were prepared from aqueous solution. Then, binder-free layered PANI/graphene nanoscale blend composite supercapacitor film was directly formed by electrophoretic deposition for the first time. Raman

spectra, Fourier transform infrared (FT-IR) spectra and X-Ray photoelectron spectroscopy (XPS) were jointly used to confirm strong π-π electron and hydrogen bond interaction in the nanosheets. Thus, because of the synergistic effects between PANI and graphene, the layered graphene/PANI composite film shows an excellent gravimetric capacitance of 384 F g^{-1} at a current density of 0.5 A g^{-1} that outperformed many other hybrid supercapacitors reported to date. The binder-free layered film also maintained up to 84 % of its capacity over 1000 cycles at a current density of 2 A g^{-1}.

Experimental section

Aniline monomers (Beijing Chemical Co.) were distilled twice under reduced pressure before use. Flake graphite was purchased from Qingdao Haida Graphite Company. All other chemicals were of analytical reagent grade and used as purchased without further treatment. Deionized water was applied for aqueous solutions or dispersions.

Sandwich-structured PANI/graphene/PANI nanosheets were synthesized simply as described as follows. Initially graphite oxide (GO) was prepared by modified Hummers method [15]. The freshly prepared GO was added into deionized water and sonicated for 2h to get a clean and well-dispersed solution with a concentration of 1 mg/mL. For the preparation of PANI/graphene composites with intimate electrochemical contact between PANI and graphene, relatively high volume of GO solution was used. To a certain volume (30 mL and 300 mL) solution, 0.93 g aniline monomers dissolved in 10 mL of 1 M HCl solution was dropwise added and stirred at 200 r/min for 1 h under 4 ℃. The solution was then further sonicated (200 W, 40 KHz) and, after 30 min, 25 mL of 0.5 M ammonium peroxydisulphate solution was added. The color of the solution gradually turned from green to black, indicating a good initiation of polymerization. After continuous sonication for 2 h, 50 mL of hydrazine hydrate (30%) were added and then the solution was sonicated for another 8 h. Because the hydrazine can reduce GO and emeraldine salt simultaneously [17], 20 mL of 1 M HCl solution containing 0.2 g of ammonium peroxydisulphate were again added to the system and stirred overnight for converting the reduced-leucoemeraldine PANI to its highly conductive emeraldine base state. The composites were collected by filtration, then washed with 0.1 M HCl followed by deionized water and finally methanol to remove the oligomers. The final composites were dried at 60 ℃ in a vacuum oven. The composites prepared from 30 mL and 300 mL GO solution were named as PG30 and PG300 respectively. Similar preparation process was used to prepare PANI nanoparticle dispersed aqueous solution. 20 mL hydrazine hydrate was added into 300 mL GO solution to prepare graphene.

The binder-free layered graphene/PANI composite film was prepared by electrophoretic deposition from aqueous solution containing PANI/graphene/PANI nanosheets. Briefly, 0.5 g PANI/graphene composites were added into 200 mL deionized water and sonicated for 2h to get a well-dispersed solution. Electrophoretic deposition was carried out at the voltage of - 20 V on nickel alloy plate (Hastelloy C-22, Haynes International, Inc.) and the deposition time was 20 min. After the layered graphene/PANI composite film was dried in air, it was pressed to increase adhesion strength and then dried under vacuum at 60 ℃ for 24 h. Electrophoretic deposition method was also used for the preparation of PANI film on nickel plate. Graphene paper was prepared by filtration of the graphene suspension.

The morphology and microstructure of the sandwich-structured PANI/graphene/PANI nanosheets and layered graphene/PANI composite film were characterized by scanning electron microscopy (SEM, FEI Helios Nanolab 600i), transmission electron microscopy (TEM, Hitachi H-7650) and atomic force microscopy (AFM, Bruker, Dimension Icon). Zeta potential was measured on a Zetasizer Nano Series 90 at 25℃, using a DTS 1060C disposable capillary cell (Malvern Instruments). The crystalline structures of the materials were investigated by a Japan Rigaku DMax-rb rotation anode X-ray diffractometer equipped with graphite monochromatized Cu Ka radiation (0.15418 nm). The content of the PANI and decomposition performance were determined thermogravimetrically using a TGA analyzer (Netzsch STA449F3) at a ramp rate of 10℃ min^{-1} in nitrogen atmosphere. FT-IR spectra were recorded on a FT-IR system (Perkin Elmer Spectrum100) from 4000 - 400 cm^{-1}. Raman spectra were recorded with a spectrophotometer (JY Co. LABRAM-HR) with operating wavelengths of 458 nm. X-Ray photoelectron spectroscopy (XPS) studies were conducted with a PHI 5700 ESCA System using Al Ka radiation (1486.6 eV).

Cyclic voltammetry (CV) was performed by a CHI660C workstation (Shanghai Chenhua, China) with a scan range of -0.2 to 0.8 V. 1 M H_2SO_4 solution was used as the electrolyte. Nickel alloy plate loaded active materials, platinum foil and Ag/AgCl electrodes were used as the working, counter and reference electrodes, respectively. Galvanostatic charge/discharge testing was performed in a two-electrode system by a Land Battery workstation (Wuhan Land, China). The test capacitor cell was fabricated by sandwiching a filter paper soaked with 1 M H_2SO_4 solution between two working electrodes. Graphene paper was attached nickel alloy sheet for testing.

In the two-electrode system, the specific capacitance (C_s) of the active electrode materials can be calculated from the discharge curve according to the following equation [20,21]:

$$C_s = 2I\Delta t /(m\Delta V) \quad (1)$$

where I, m, ΔV and Δt represent the discharge current (A), the mass of the active electrode materials (g) on single side, the voltage range (V) and the discharge time, respectively. The specific capacitance can also be calculated from the CV curves[25]:

$$C_s = (\int I dV)/(vmV) \quad (2)$$

where I is the response current (A), V is the potential (V), v is the potential scan rate (V s^{-1}), and m is the mass of the electroactive materials in the electrodes (g).

Results and discussion

GO can form stable suspension in water, thus a homogeneous mixture of GO in acidic solution containing aniline monomers can be easily obtained. Moreover, the oxygen functional groups on the surface of GO providing compatibility with PANI during the in situ polymerization [17,22]. In addition, the π-π stacking force between the phenyl and basal planes of GO was also beneficial to *in situ* polymerization occurring on the surface of GO [19]. The fabrication of sandwich-structured PANI/graphene/PANI nanosheets essentially includes three substeps, as illustrated in Fig. 1.

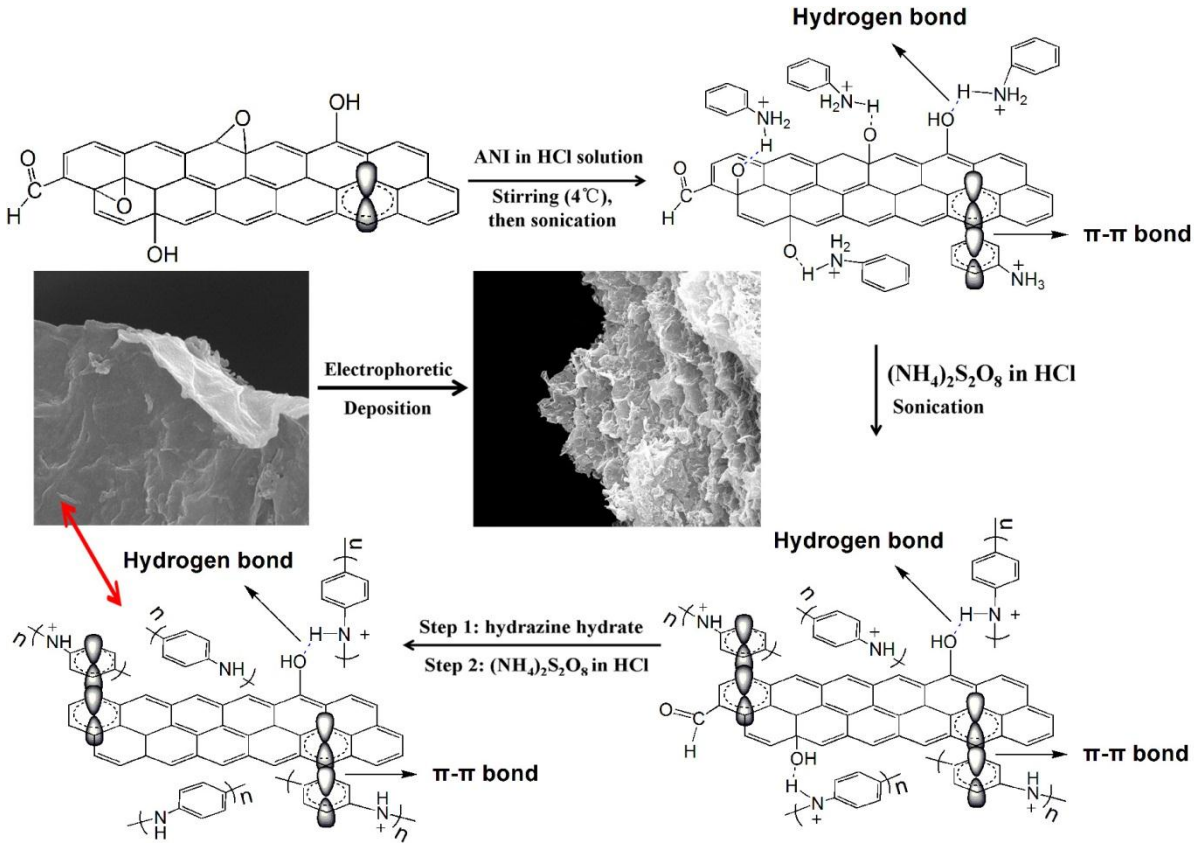

Fig. 1. A schematic illustrating the preparation process of sandwich-structured PANI/graphene/PANI nanosheets, with SEM pictures of the sample.

Initially, acidic solution containing aniline monomers is added into GO well-dispersed aqueous solution. Aniline in HCl solution gets one proton to be anilinium cation, thus the π-π stacking force and hydrogen bond between the anilinium cation and GO nanosheets facilitate the uniform adsorption of protonated aniline molecules under stirring. The stirred solution is further sonicated. It is known that there are plenty of epoxy groups on the GO surface [32,33]. The high temperature and pressure from the collapse of acoustic cavitations introduced by ultrasonic vibration cause the cleavage of epoxy groups [31,34]. The active oxygen atoms from broken epoxy groups further attract more protonated aniline molecules on the GO surface by hydrogen bond. Subsequent sonication and addition of ammonium peroxydisulphate make the aniline monomers polymerized, while the epoxy groups are reduced with the elimination of neutral water molecules [31]. The composites are then treated with hydrazine. Most of GO are believed to be reduced to form conductive graphene sheets [17]. However, the PANI may also be reduced from emeraldine base state to the leucoemeraldine state during the reduction process [17]. To convert the leucoemeraldine to emeraldine, a supplemental amount of ammonium peroxydisulphate in HCl solution is added and stirred. HCl solution is further used to re-dope the PANI. Finally, the oligomers in the composites are removed by methanol. The resultant composites glows a darkgreen color under ambient room light (see Fig. S1a in the ESI) and the PG300 can be easily dispersible in water to be a homogeneous dispersion of individual nanosheet (see Fig. S1b in the ESI). On a whole, unlike other graphene/PANI composite preparation methods in which oxygen containing functional groups were only used as nucleation sites, our preparation strategy used almost all the oxygen functional groups (especially the epoxy groups), thus the whole surface of graphene sheet was uniformly covered by PANI film.

The typical micromorphologies of the resulting GO and the PANI/graphene/PANI nanosheets were investigated by SEM and TEM. Fig. 2a and Fig. 2b show the SEM images of PG30 and PG300 respectively. In the case of PG30, besides some PANI/graphene/PANI nanosheets (the arrows point), plenty of polyaniline particles are observed due to an excess of aniline molecules. Contrarily, the SEM images of PG300 only show thin nanosheets with typical flat and relatively rough surface, indicating the surface of graphene is uniformly covered by ultrathin PANI film. Furthermore, as shown in Fig. 2S, no pure PANI particles are found in the PG300. Such kind of nanoscale uniform blend of graphene with PANI predicts a highly effective use of active surface area of the graphene sheet and intimate electrochemical interface. In addition, compared to the nanosheets of PG30, the thickness of the nanosheets in PG300 is much thinner, thus the interaction between PANI and graphene in PG300 must be stronger than that in PG30, which may lead the PG300 exhibits better electrochemical properties. Finally, the existence of continuous ultrathin polyanilne film on the graphene confirms that the epoxy groups play an important role during polymerization, because when the oxygen containing functional groups act as nucleation sites, only nanoparticles or nanorods were prepared on the graphene surface [17,18,22]. To obtain further

insight into the morphology of composite as well as the mechanism of PANI polymerization on GO surface, transmission electron microscopy (TEM) is used. TEM image of GO performs a transparent layered and crumpled structure morphology of the sheets (Fig. 2c), and this structure morphology is derived from the existence of sp^3-hybridized carbon atoms introduced by chemical oxidation exfoliation [15]. Further, as concluded from the SEM image, overmuch aniline molecule in solution make the loaded absorption of anilinium cations on GO surface excessive, finally leading to overloaded PANI on the surface (Fig. 2d). Interestingly, the PANI/graphene/PANI sheets of PG300 show a slightly higher contrast than that of GO, indicating the coating of ultrathin PANI film on the graphene surface (Fig. 2e). A higher-magnification TEM image of PG300 nanosheet is taken to investigate the morphology of PANI on graphene (Fig. 2f). It is clear to see that the whole surface of graphene is uniformly covered by PANI.

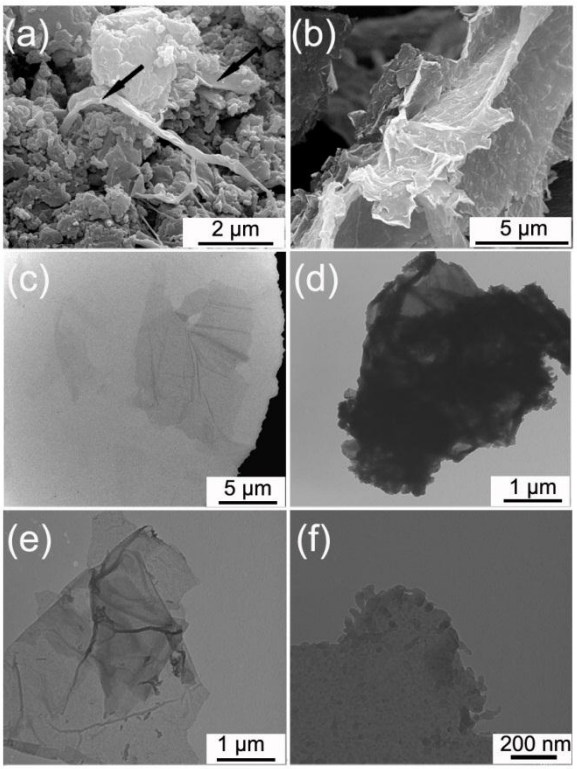

Fig. 2. Typical SEM images of (a) PG30, and (b) PG300. TEM images of (c) GO, (d) PG30, (e) PG300, and (f) a higher-magnification of PG300. Arrows in image (a) denote the sandwich-structured PANI/graphene/PANI nanosheets.

Atomic force microscopy (AFM) analysis is another direct way to investigate the surface structure and thickness of the as-prepared composite nanosheets. Fig. 3a and Fig. 3b present the AFM images of GO and PG300 respectively. It is clear to find that the polymerization of aniline has no significant impacts on the nanosheet shape of GO and the polyaniline rather uniformly covers the graphene surface. Further, the PG300 performs an average height of *ca.* 8.9 nm *vs. ca.* 1.5 nm of GO, namely, a thickness of 3.7 nm polyaniline films on the each side of graphene.

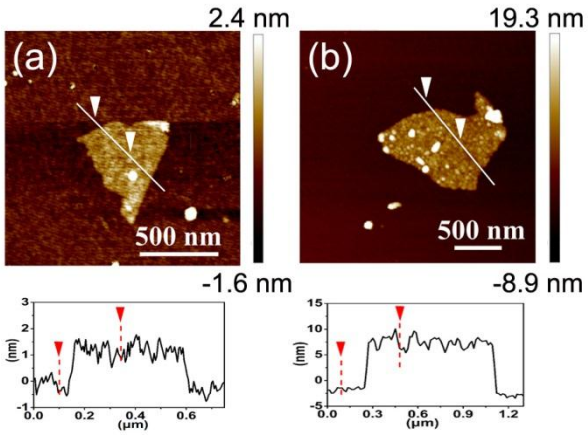

Fig. 3. AFM images of (a) GO, and (b) PG300.

Raman scattering is used to study the graphene/PANI composites. As shown in Fig. 4a, significantly componential changes occur after the coating of PANI on the graphene sheets. The GO displayed two prominent peaks at 1530 and 1580 cm^{-1}. The former peak corresponds to D mode derived from the existence of sp^3-hybridized carbon, while the latter one is assigned to G mode which is related to the vibration of a sp^2-hybridized carbon. As expected, in the composites, three new representative shoulders are observed at 1174, 1487 and 1607 cm^{-1}, which correspond to C–H bending deformation in the quinoid/phenyl groups, C=N stretching vibration of the quinonoid units and C–C stretching deformations in benzoid ring of PANI, respectively [7,35]. The significantly decreased intensity of C–H bending deformation of quinoid/phenyl groups in graphene/PANI composite may be caused by the intimate electron interaction between conjugated PANI and graphene. Since the aromatic/quinoid structure in PANI is known to interact strongly with the plane of carbon nanotube surfaces via π-stacking [35,36], similar situation may occur in the graphene/PANI composite, leading to the restriction on the C–H bending deformation of quinoid/phenyl groups. It is also interesting noting that the 2D band of graphene became apparent in the graphene/PANI composite. From the 2D band of the graphene/PANI composite spectra, it appears that each individual graphene is coated by PANI and no aggregation of graphene sheets occurs [37-39].

In conjunction with Raman spectrum, FT-IR spectroscopy is used to get more insights into the chemical bond structure. As can be seen in Fig. 4b, the FT-IR spectrum of GO shows a strong absorption band at 3407 cm^{-1} due to the stretching of O−H groups associated with the interlayer water molecules and the absorption band at 1624 cm^{-1} is also attributed to the vibrations of the water molecules. The peak at 1734 cm^{-1} is assigned to the C=O stretching in the –COOH groups. Absorption bands assigned to carboxy(C-O; 1392 cm^{-1}), epoxy(C-O; 1217 cm^{-1}), and alkoxy(C-O; 1062 cm^{-1}) groups situated on the surface of GO sheet are also detected [15]. However, no absorption peaks corresponding to the oxygen containing functional groups are found in the graphene/PANI composites, indicating the majority of such groups disappear due to the reduction of the hydrazine [17]. Compared with GO, a group of typical bands corresponding to the PANI appear in the spectra of graphene/PANI composites, C=C stretchings of the quinonoid rings and benzenoid rings at

1561 cm^{-1} and 1475 cm^{-1} respectively. And the peak of C-N stretching of secondary aromatic amines occur at 1301 cm^{-1}, while the peak at 1243 cm^{-1} can be assigned to the C-H bendings of the benzenoid ring and the quinonoid ring [7]. The relative strength of peak intensities between quinonoid ring (1561 cm^{-1}) and benzenoid ring (1475 cm^{-1}) is very similar both in PG30 and PG300, which reflected the oxidized situation of PANI in these two composites is similar. And the ratio of the peak intensities of quinoid to benzenoid stretchings in graphene/PANI composite is ca. 0.85 (0.85 for PG30 and 0.86 for PG300), indicating the PANI of the graphene/PANI is very close to the emeraldine salt state [40]. The absorption band at 1140 cm^{-1} is related to the doping effects of graphene fragments on the PANI backbone, which indicates both a charge transfer process and an interaction of the graphene fragments with the PANI quinoid rings [19,35,36]. Thus, the intensified absorption of this band presented a more intimate interaction between PANI and graphene in PG300 than in PG30.

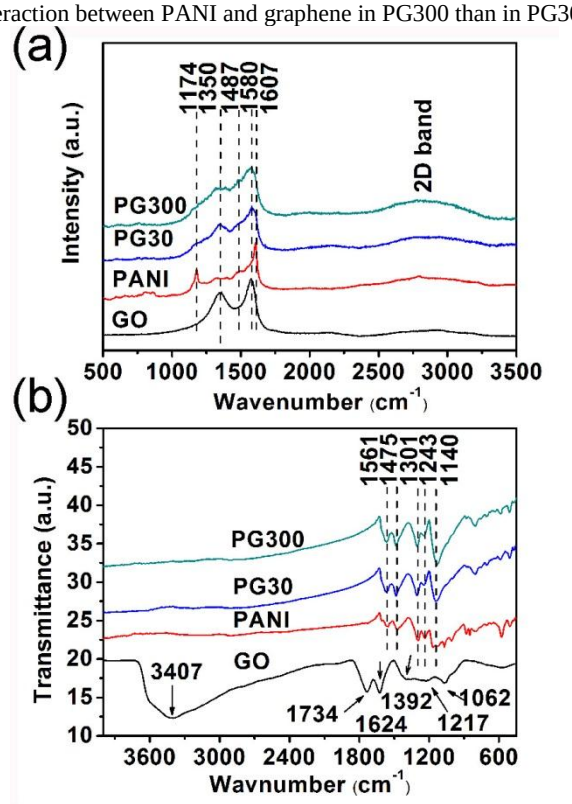

Fig. 4. (a) Raman spectra and (b) FT-IR spectra of the samples.

Meanwhile, X-ray photoelectron spectroscopy (XPS) is used to probe the different electronic structures and chemical bond information of as-prepared materials. Fig. 5a shows the wide-range spectra of the obtained GO, pure PANI and graphene/PANI composites. It is evident to observe that the GO exhibits a considerable degree of oxidation and subsequent reduction treatment of hydrazine results in a certainly low oxygen extent in the final compound. Reduction treatment of GO removes the oxygen atoms and increases the sp^2-hybridized carbons [7], leading to the increase of the π electron cloud stacking between graphene and aromatic/quinoid structure in PANI [35,36], which may facilitate the electron transfer and enhance electrochemical properties of the composite materials. The presence of N1s in the graphene/PANI composites indicates that PANI is deposited onto graphene surface. In addition, the appearance of a chloride peak in the XPS spectra shows clearly that pure PANI and PANI in graphene/PANI composites were both doped with Cl^-. To further determinate the chemical bond state of carbon in graphene/PANI composites, the comparison of the C1s core level of GO (Fig. 5b) and PG300 (Fig. 5c) was made. The C1s of XPS spectrum of GO (Fig. 5b) can be deconvoluted into three Gaussian peaks at 284.5 eV, 286.9 eV and 288.5 eV, attributed to the typical signals of C=C, C-O (hydroxyl and epoxy groups) and C=O (carboxyl groups), respectively [7]. Meanwhile, the detected carbon element in the graphene/PANI composite mainly originates from PANI, which is revealed from the C=C band at 284.8 eV and C–N band at 285.4 eV of the core-level C1s XPS spectrum [17]. However, it is worthy to note that there remains a weak C-O band at 287.2 eV, which may be assigned to the residual hydroxyl or epoxy groups on the graphene sheets. Such residual groups may form hydrogen bonds with the polyaniline [41,42], and then bring another intimate interaction between graphene and PANI besides the π-π electron stacking [24,43,44]. The N1s core level of PG300 (Fig. 5d) is detected to reveal the oxidized state of PANI in composites. The asymmetric N1s core level of PG300 is composed of four subpeaks centered at about 389.6 eV (=N-), 399.4 eV (-NH-), 400.2 eV (-NH^+=) and 402.1 eV (-NH_2^+-) [9,22], respectively. The area fraction of these four peaks is 0.36, 0.29, 0.17 and 0.18, respectively, where the total area from protonated nitrogen atoms is 35%, indicating that the doping level of polyaniline in PG300 was 35%.

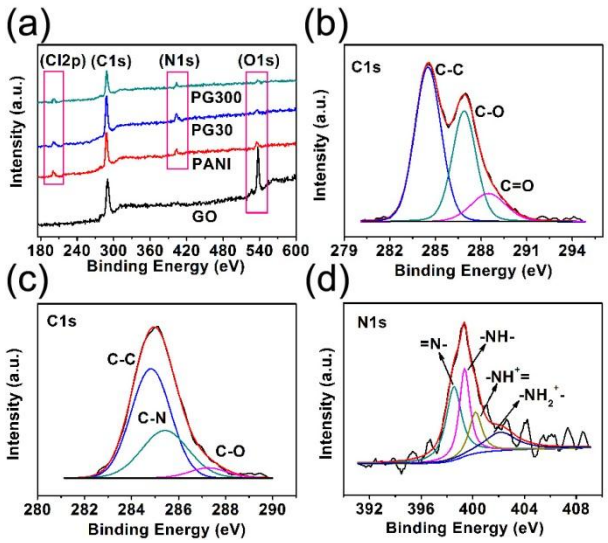

Fig. 5. XPS spectra of (a) GO, pure PANI, PG30, and PG300; (b) the C1s region of GO, (c) the C1s region of PG300, (d) the N1s region of PG300.

X-ray diffraction (XRD) patterns of the powder samples are taken in order to analyze the crystalline structure of composites that can be quantitatively estimated from the peak position and the relative peak intensity. Fig. 6a exhibits the XRD pattern of the as-prepared GO, demonstrating an intense and sharp peak centered at 2θ = 11.6 °, corresponding to the interplanar spacing of GO sheets. This peak can be assigned to the (001) crystal planes, while the interplanar spacing usually depends on the

preparation method and the number of water molecules inserted in the gallery space of materials [17]. In the case of graphene/PANI composites, the intrinsic peak of GO disappear, indicating the GO sheets have almost been reduced and no aggregation. Additionally, it is well-documented that the graphene exhibits diffraction peaks at 2θ = ca. 25 ° and ca. 48 ° due to graphite-like structure [45], the broad nature of reflection peaks and disappearance of diffraction peaks of graphene indicates poor ordering of the sheets along the stacking direction in the composites, implying graphene sheets could have been completely separated and covered by PANI thin film. The pure PANI powder sample exhibited a broad reflection peaks, with the intense peaks at 2θ =20.6 ° (i.e., d=0.43 nm) and 25.4 ° (i.e., d=0.35 nm), corresponding to the (020) and (200) crystal planes of PANI. These reflection peaks belong to emeraldine salt form PANI and indicate some crystalline order in the bulk PANI powder sample [46,47]. However, the graphene/PANI composites present a different crystalline structure from pure PANI powder. The intensity of diffraction peak at 2θ = 25.4 ° becomes comparable, even larger than that of the peak at 2θ = 20.6 °, indicating GO surface plays an important role during the growth of PANI on its surface and (200) crystal plane are more favorable in the view of energy during polymerization process. Besides this two peaks, a new low-intensity peak at 2θ = 15.2 °corresponding to (011) crystal planes of emeraldine salt state PANI is found [46,47], which further indicates the influence of GO on the growth of PANI during polymerization. Moreover, the reason for the relatively low intensity of diffraction peaks assigned to (200) crystal planes and (011) crystal planes in PG30 may result from the existence of PANI particles in the composite, as also evidenced from the SEM examination. The X-ray diffraction spectrum of PANI particles overlaps on the diffraction spectrum of PANI/graphene/PANI sheets, leading these peaks to be not obvious. Interestingly, for the graphene/PANI composite, a weak peak can be observed nearly at 2θ = 9.3 °, which is much lower than that of GO. Similar results are also observed in other authors' research [15,17], and it implies the interplanar spacing of the graphene/PANI composite is broadened due to possible intercalation of PANI and that the PANI/graphene/ PANI sheets are completely separated by treatment with PANI thin film [15]. Therefore, the XRD measurement further confirms the formation of PANI/graphene/PANI sheets. And the result is consistent with that of morphological measurement, Raman and FT-IR investigations. To get further information about the composition of the graphene/PANI composites, the comparison of mass losses upon heating in nitrogen atmosphere is determined thermogravimetrically.

Fig. 6b shows the thermogravimetric (TGA) analysis of GO, pure PANI and the graphene/PANI composites samples. The GO shows thermal instability as reported in the literatures [15,31]. The roughly 20% of weight loss before 150 ℃ can be attributed to desorption of water molecules and other residual chemicals. The oxygen containing functional groups lead GO to exhibit pyrolysis at around 250℃, leading to a major weight loss of ca. 45%. As for PANI powder, it exhibits typical thermal behavior [17]. The initial weight loss around 100℃ is caused by desorption of H_2O and the following weight loss is due to the decomposition of PANI. In the case of graphene/PANI composites, the thermal stability is remarkable enhanced due to the deposited PANI on the graphene layers. For instance, the PG30 and PG300 show 22% and 19% weight loss at 450℃, however 30% weight loss occurred in pure PANI at same temperature. Interestingly, the graphene/PANI composite powders exhibit similar thermal behavior to the pure PANI powder, implying the reduction of GO to graphene in composites, due to the fact that the reduced GO is rather thermal stable in the nitrogen atmosphere below 1000℃ [48]. Furthermore, the reason why PG30 presents relatively lower thermal stability than PG300 may be in the composition of composites. More PANI particles in PG30 lead to higher thermal instability.

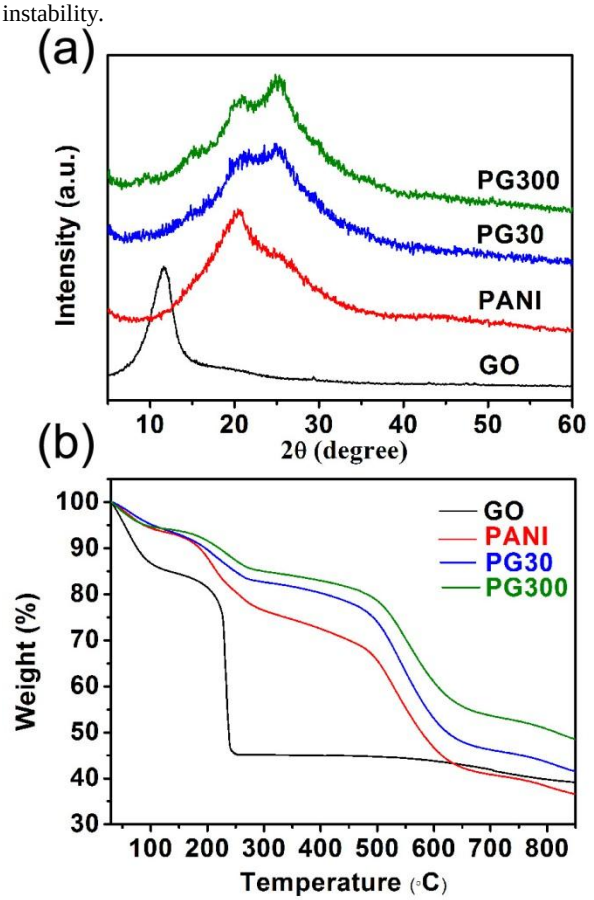

Fig. 6. (a) XRD patterns and (b) TGA thermograms of the samples.

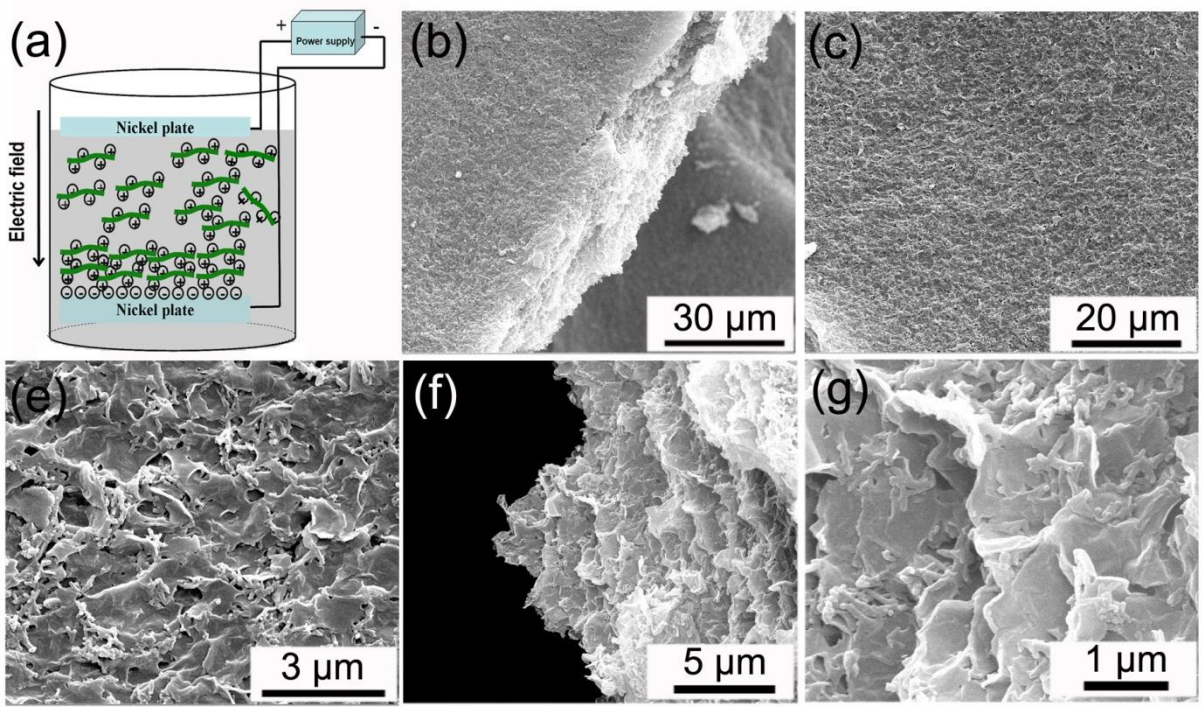

Fig. 7. (a) Sketch of electrophoretic deposition for the preparation of a layered polyaniline/graphene film. (b) SEM image of an as-deposited film with fracture surface. (c)(d) SEM images of the film surface. (e)(f) SEM images of the fracture surface.

Table 1. Zeta potentials of the different samples

Sample name	GO	Graphene	Pure PANI	GP30	GP300
Zeta potential (mV)	-41.6	-8.7	24.3	22.5	28.2

Typically, emeraldine base state PANI nanoparticals carry positive charge, which makes them dispersible in aqueous solution [9]. The zeta potentials of the GO, graphene, pure PANI, PG30 and PG300 suspensions are listed in Table 1. The zeta potential of graphene is significantly higher than that of GO, due to the reduction effects of hydrazine. However, it was still negative, which indicates that there is remaining oxygen containing groups on the graphene sheets, consistent with the result of XPS examination on PG300. Moreover, compared to the negatively charged graphene, all the graphene/PANI composites are positively charged, which indicates the coverage of PANI on graphene surface. With the homogeneous suspensions, we fabricate the binder-free layered graphene/PANI composite film by a cathodic electrophoretic deposition method (Fig. 7a). To make the deposition more easily and effectively, the electrodes were parallel to the solution surface. Fig. 7b-7f shows the SEM top-view images of grahene/PANI composite film based on GP300 and Fig 3S exhibited its cross-section SEM images. While the SEM images of grahene/PANI composite film of GP30 are presented in Fig. S4 (these two films are also called as PG300 and PG30.).

As shown in Fig. 7b, the deposited grahene/PANI composite film from GP300 exhibits a porous and flat surface, indicating that the electric-field-induced deposition progress of PANI/graphene/PANI sheets is in a uniform way. The thickness of PG300 is about 13.3 μm (Fig. 3Sa). Fig. 7c and 7d exhibit the surface of as-deposited film with different magnification. It is observed that the sheets are closely attached each other, thus leading to the formation of an interconnected network which can facilitate the motion of electrons during electrochemical reaction. In addition, the presence of small holes allows the facile penetration of electrolyte in the film. The fracture surface of the film is further clearly shown in Fig. 7e and 7f. It is found that the PANI/graphene/PANI sheets are assembled in a highly ordered way along the perpendicular direction, and are attached each other tightly, which can be further confirmed in Fig. 3Sb. The grahene/PANI composite film from GP30 presents a different surface morphology (Fig. S4). Because of the coexistence of PANI particles and PANI/graphene/PANI sheets in the aqueous solution, PANI particles (circle "A") and PANI/graphene/PANI sheets (circle "B") are co-deposited on the nickel plate (Fig. S4a). The loosely stacked graphene/PANI sheets and PANI particles can not provide an effective network for the electron transportation during the electrochemical reaction. More clear clarification about the surface is shown in Fig. S4b, in which is the surface SEM image at a defective surface part. The nanomaterials arrows pointed are PANI/graphene/PANI sheets, meanwhile others are PANI particles. The deposited PG300, PG30, pure PANI and graphene paper are *ca.* 1.42 mg cm^{-2}, 0.83 mg cm^{-2}, 2.57 mg cm^{-2}, and 25.31 mg cm^{-2}, respectively.

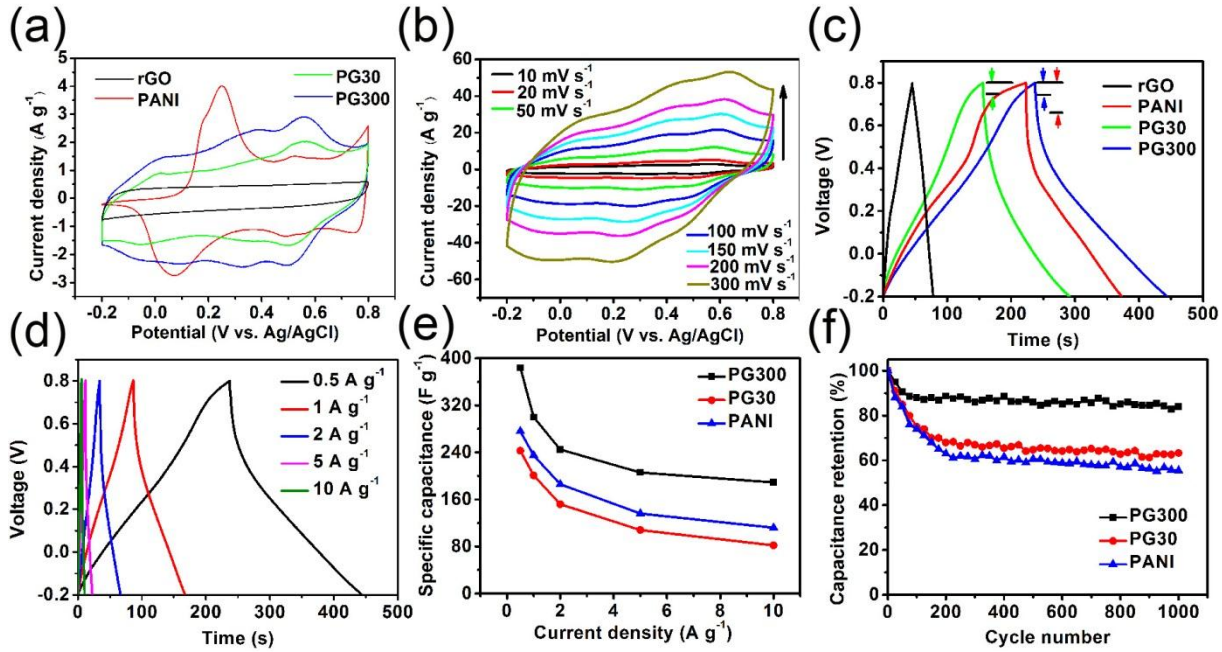

Fig. 8. (a) CV curves of PG300, PG30, pure PANI and graphene paper at 10 mV s^{-1} in 1 M H_2SO_4. (b) CV curves of PG300 at different scan rates. (c) Galvanostatic charge/discharge curves of PG300, PG30, pure PANI, and graphene paper at a current density of 0.5 A g^{-1}. (d) Galvanostatic charge–discharge curves of PG300 at different current densities. (e) Variation of the specific capacitance with current density for PG300, PG30, and pure PANI. (f) Cycle stability of PG300, PG30, and pure PANI measured at a current density of 2 A g^{-1}.

Cyclic voltammetry (CV) studies in Fig. 8a are performed to analyze the capacitance behavior of graphene, pure PANI and layered graphene/PANI composite film with a potential window from -0.2 to 0.8 V *versus* Ag/AgCl at a scan rate of 10 mV s^{-1} in 1M H_2SO_4 solution. The CV curve of the graphene is nearly rectangular with no obvious peaks, which is typical for the electric double-layer capacitance of carbon-based materials [14]. However, the occurrence of redox peaks in the pure PANI and graphene/PANI composites indicates the presence of pseudocapacitive PANI [17]. It is worthy to note that the CV curve integrated area of layered graphene/PANI film from PG300 is larger than that of other three materials at the same scan rate, suggesting its higher specific capacitance. Further, the CV curves of composite films become more alike to the rectangular shape, indicating the important role of graphene for the capacitance of composites. Moreover, Fig. 8b shows the detailed CV behaviors of the PG300 film at different scan rates from 10 to 300 mV s^{-1}. The cathodic peaks and anodic peaks have shifted slightly, which indicates fast electrochemical reaction speed during redox reactions. Thus, it is reasonable to conclude that this layered PANI/graphene film is a promising candidate for supercapacitor.

To reveal the electrochemical capacitive performance of these electrode materials, galvanostatic charge/diacharge are performed at a current density of 0.5 A g^{-1}, as shown in Fig. 8c. The graphene paper exhibits a triangular-chape charge/discharge curve, indicating that it is an EDLC capacitor. However, the charge/discharge plots of PG30 and PG300 show a capacitive behavior with almost symmetric curves, where the deviation to linearity is due to the pseudocapacitive nature of PANI [21]. Furthermore, the "IR drop" of the PG30 and PG300 is lower than that of PANI, which reflects that the graphene/PANI composites possesses lower internal resistance compared to the pure PANI [20, 21]. The specific capacitance of the PG300 electrode is 384 F g^{-1}, which is much higher than that of the PG30 electrode (247 F g^{-1}), the pure PANI electrode (276 F g^{-1}) and the graphene paper (69 F g^{-1}). Without consideration of the synergistic effects between PANI and graphene, the theoretical capacitace of PG300 electrode is 214 F g^{-1} (17.9% × 69 F g^{-1} + 82.1% × 276 F g^{-1}). Thus, the enhanced capacitance is as high as 170 F g^{-1}, indicating the key effects of the interactions between the PANI and the graphene on improving the capacitive behavior. The enhanced pseudocapacitive performance in PG300 can be attributed to the following three factors. First, the PANI film covering on graphene has a thickness of 3.7 nm, which greatly reduces the ionic diffusion path and increases the utilization of PANI as an electrode material. Second, the intimate interactions between the grahene and the PANI, including the strong π-π electron and hydrogen bond interaction, facilitate the electron transfer process during the redox reactions [19,21,24]. Third, the embedded graphenes can act as the conducting pathways which are beneficial for the electron transport [15]. The specific capacitance of the layered graphene/PANI composite (PG300) is similar to the elaborately controlled layer-by-layer (LbL) assembled PANI/graphene composite film (375.2 F g^{-1} at 0.5 A g^{-1})[25], and also higher than

several recent studies of hybrid PANI and graphene structures, such as the free-standing graphene/PANI composite paper prepared by the electrodeposition of PANI into graphene paper (233 F g^{-1} at 20 mV s^{-1} by CV *vs* 324 F g^{-1} from our study) [16], the free-standing rGO/PANI-nanofiber film prepared by vacuum filtration (210 F g^{-1} at 0.3 A g^{-1}) [23], the polyaniline-grafted reduced graphene oxide composites (250 F g^{-1} at 100 mV s^{-1} by CV *vs* 275 F g^{-1} from our study) [15], the graphene/PANI nanofiber composites (200 F g^{-1} at 0.5 A g^{-1}) [17], the microspherical polyaniline/graphene nanocomposites (261 F g^{-1} at 0.5 A g^{-1}) [18], the negatively-charged poly(sodium 4-styrenesulfonate) mediated graphene/PANI composite paper (301 F g^{-1} at 0.5 A g^{-1}) [49], the flexible 3D graphene oxide/carbon nanotube/polyaniline composite paper (202 F g^{-1} at 0.5 A g^{-1}) [50], and the PANI directly coated reduced graphene oxide sheet composites (349 F g^{-1} at 0.5 A g^{-1}) [51]. More comparison about the specific capacitance of PG300 with literature data can be found in Table S1 in ESI.

For further comparison about the capacitive properties of PG30, PG300 and PANI, the capacitance of these materials at different current densities of 0.5 - 10 A g^{-1} are investigated. Fig. 8d presents the charge-discharge properties of PG300 at different current, while Fig. S5a and Fig. S5b show relevant properties in PANI film and PG300. And the variations of the spesific capacitance with the current density of these three electrode materials were plotted together in Fig. 8e for obvious comparisons. It is noted that the specific capacitance decreases with the increase of the current density. For PG300, the specific capacitance decreases from 384 to 312 F g^{-1} as the current density increases from 0.5 to 1 A g^{-1}, and the capacitive retention is 81%. The specific capacitance of PG300 film at 1 A g^{-1} (312 F g^{-1}) is also larger than some binder-free graphene/PANI capacitor electrodes, such as the LBL assembled PANI/graphene composite film (*ca.* 225 F g^{-1} at 1 A g^{-1})[25], free-standing rGO/PANI-nanofiber film prepared by vacuum filtration (202 F g^{-1} at 1 A g^{-1}) [23] and flexible 3D graphene oxide/carbon nanotube/polyaniline composite paper (181 F g^{-1} at 1 A g^{-1}) [50]. Even when the current density is as high as 10 A g^{-1}, 50% (192 F g^{-1}) of the specific capacitance is maintained. However, when a current density of 0.5 to 1 A g^{-1} is applied to the other two electrodes, an acceptable retention is received (82% for PG30 and 85% for pure PANI), but only 34% and 41% of the specific capacitance are obtained for PG30 and pure PANI, respectively, when 10 A g^{-1} of current density is used. These results revealed that the layered PANI/graphene film electrode (PG300) has a better sustainability and rate performance compared with the other two materials.

Another important parameter for electrochemical supercapacitor is cycling performance. As exhibited in Fig. 8f, the PG300 electrode performs better than other two materials. After 1000 cycles, 84% of initial capacitance retains at a discharge current density of 2 A g^{-1}, compared to only 65% for PG30 and 55% for PANI. Comparison about the cycling performance of PG300 with literature data can be found in Table S2 in ESI. The intimate π-π electron and hydrogen bond interaction between polyaniline and graphene may facilitate the electron transportation during redox reactions, which makes the materials more stable. Moreover, the graphene sheets embedded in PANI may restrict the volume change during insertation/deinsertation process, thus further improves the stability [7, 22].

Conclusions

In summary, we have demonstrated a facile and green way to prepare sandwich-structured PANI/graphene/PANI nanosheets with covering ultrathin PANI film (3.7 nm). Then, a binder-free layered PANI/graphene supercapacitor film was assembled from these nanosheets by electrophoretic deposition. Intimate electronic contact between graphene and PANI was confirmed by Raman analysis, FT-IR spectra and XPS analysis. By analyzing the TGA and XRD examination results, combination of graphene not only improved the crystallinity of PANI, but also improved its thermal stability. The layered composite film exhibits excellent gravimetric capacitance of 384 F g^{-1} at a 0.5 A g^{-1} discharge current density and maintained its capacity up to 84% over 1000 cycles at a current density of 2 A g^{-1}. In addition, this preparation method may provide a promising strategy for preparation of graphene-based composites with other conducting polymers and binder-free film electrodes. Further, these graphene/PANI sheets with sandwich structure would have promising applications in energy storage devices, solar cells, chemical sensors, semiconductor devices, *etc*.

Acknowledgements

We thank National Natural Science Foundation of China (No. 51010005, 90916020, 51174063), the Program for New Century Excellent Talents in University (NCET-08-0168), Natural Science Funds for Distinguished Young Scholar of Heilongjiang province, and the project of International Cooperation supported by Ministry of Science and Technology of China (2013DFR10630)

Notes and references

‡
[a] *Center for Composite Material, Harbin Institute of Technology, Harbin, China. Fax: 086 45186402345; Tel: 086 451 86402345; E-mail: yaoli@hit.edu.cn*
[b] *School of Chemical Engineering and Technology , Harbin Institute of Technology, 150001, Harbin, China. E-mail: jpzhao@hit.edu.cn*
[c] *Laboratory of Inorganic Materials Chemistry (CMI), University of Namur, 61, rue de Bruxelles, B-5000 Namur, Belgium.*

† Electronic Supplementary Information (ESI) available: [details of any supplementary information available should be included here]. See DOI: 10.1039/b000000x/

1 Z. Yang, J. Zhang, M. C. W. Kintner-Meyer, X. Lu, D. Choi, J. P. Lemmon and J. Liu, *Chem. Rev.*, 2011, **111**, 3577-3613.
2 R. F. Service, *Science*, 2006, **313**, 902.
3 C. Liu, F. Li, L. P. Ma and H. M. Cheng, *Adv. Mater.*, 2010, **22**, E28-E62.
4 P. Simon and Y. Gogotsi, *Acc. Chem. Res.*, 2013, **46**, 1094-1103.
5 G. Feng, S. Li, J. S. Atchison, V. Presser and P. T. Cummings, *J. Phys. Chem. C*, 2013, **117**, 9178-9186.
6 D. Wei, M. R. J. Scherer, C. Bower, P. Andrew, T. Ryhänen, and U. Steiner, *Nano Lett.*, 2012, **12**, 1857-1862.

7 H. P. Cong, X. C. Ren, P. Wang and S. H. Yu, *Energy Environ. Sci.*, 2013, **6**, 1185-1191.

8 K. S. Ryu, K. M. Kim, N. G. Park, Y. J. Park and S. H. Chang, *J. Power Sources*, 2002, **103**, 305-309.

9 H. M. Zhang, Q. Zhao, S. P. Zhou, N. J. Liu, X. H. Wang, J. Li and F. S. Wang, *J. Power Sources*, 2011, **196**, 10484-10489.

10 S. Chaudhari, Y. Sharma, P. S. Archana, R. Jose, S. Ramakrishna, S. Mhaisalkar and M. Srinivasan, *J. Appl. Polym. Sci.*, 2013, **129**, 1660-1668.

11 Z. Q. Niu, P. S. Luan, Q. Shao, H. B. Dong, J. Z. Li, J. Chen, D. Zhao, L. Cai, W. Y. Zhou, X. D. Chen and S. S. Xie, *Energy Environ. Sci.*, 2012, **5**, 8726-8733.

12 S. Park and R. S. Ruoff, *Nat. Nanotechnol.*, 2009, **4**, 217-224.

13 A. K. Geim, *Science*, 2009, **324**, 1530-1534.

14 Z. Fan, J. Yan, L. Zhi, Q. Zhang, T. Wei, J. Feng, M. Zhang, W. Qian and F. Wei, *Adv. Mater.*, 2010, **22**, 3723-3728.

15 N. A. Kumar, H. Choi, Y. R. Shin, D. W. Chang, L. Dai and J. Baek, *ACS Nano*, 2012, **6**, 1715-1723.

16 D. W. Wang, F. Li, J. Zhao, W. Ren, Z. G. Chen, J. Tan, Z. S. Wu, I. Gentle, G. Q. Lu and H. M. Cheng, *ACS Nano*, 2009, **3**, 1745-1752.

17 K. Zhang, L. L. Zhang, X. S. Zhao and J. Wu, *Chem. Mater.*, 2010, **22**, 1392-1401.

18 H. L. Cao, X. F. Zhou, Y. M. Zhang, L. Chen and Z. P. Liu, *J. Power Sources*, 2013, **243**, 715-720.

19 J. J. Xu, K. Wang, S.-Z. Zu, B.-H. Han and Z. X. Wei, *ACS Nano*, 2010, **4**, 5019-5026.

20 B. Ma, X. Zhou, H. Bao, X. W. Li and G. C. Wang, *J. Power Sources*, 2012, **215**, 36-42.

21 M. K. Liu, Y.-E. Miao, C. Zhang, W. W. Tjiu, Z. B. Yang, H. S. Peng and T. X. Liu, *Nanoscale*, 2013, **5**, 7312-7320.

22 H. L. Wang, Q. L. Hao, X. J. Yang, L. D. Lu and X. Wang, *Nanoscale*, 2010, **2**, 2164-2170.

23 Q. Wu, Y. X. Xu, Z. Y. Yao, A. R. Liu and G. Q. Shi, *ACS Nano*, 2010, **4**, 1963-1970.

24 J. H. Liu, J. W. An, Y. C. Zhou, Y. X. Ma, M. L. Liu, M. Yu and S. M. Li, *ACS Appl. Mater. Interfaces*, 2012, **4**, 2870-2876.

25 T. Lee, T. Yun, B. Park, B. Sharma, H.-K. Song and B.-S. Kim, *J. Mater. Chem.*, 2012, **22**, 21092-21099.

26 H. Bai, Y. Xu, L. Zhao, C. Li and G. Shi, *Chem. Commun.*, 2009,1667-1669.

27 J. L. Xiang and L. T. Drzal, *Polymer*, 2012, **53**, 4202-4210.

28 Y. Lu, Y. Song and F. P. Wang, *Mater. Chem. Phys.*, 2013, **138**, 238-244.

29 G. Q. Wang, W. Xing and S. P. Zhuo, *Electrochim. Acta*, 2012, **66**, 151-157.

30 C.-Y. Liu, K.-C. Huang, P.-H. Chung, C.-C. Wang, C.-Y. Chen, R. Vittal, C.-G. Wu, W.-Y. Chiu and K.-C. Ho, *J. Power Sources*, 2012, **217**, 152-157.

31 D. Majumdar, M. Baskey and S. K. Saha, *Macromol. Rapid Commun.*, 2011, **32**, 1277-1283.

32 Z. Li, W. Zhang, Y. Luo, J. Yang and J. G. Hou, *J. Am. Chem. Soc.*, 2009, **131**, 6320-6321.

33 D. Pan, J. Zhang, Z. Li and M. Wu, *Adv. Mater.*, 2010, **22**, 734-738.

34 E. B. Flint and K. S. Suslick, *Science*, 1991, *253*, 1397-1399.

35 M. Baibarac, I. Baltog, C. Godon, S. Lefrant and O. Chauvet, *Carbon*, 2004, **42**, 3143-3152.

36 H. Zengin, W. S. Zhou, J. Y. Jin, R. Czerw, D. W. Smith, L. Echegoyen, D. L. Carroll, S. H. Foulger and J. Ballato, *Adv. Mater.*, 2002, **14**, 1480-1483.

37 A. C. Ferrari, J. C. Meyer, V. Scardaci, C. Casiraghi, M. Lazzeri, F. Mauri, S. Piscanec, D. Jiang, K. S. Novoselov, S. Roth and A. K. Geim, *Phys. Rev. Lett.*, 2006, **97**, 187401.

38 Z. H. Ni, Y. Y. Wang, T. Yu and Z. X. Shen, *Nano Res.*, 2008, **1**, 273-291.

39 D. Graf, , F. Molitor, K. Ensslin, C. Stampfer, A. Jungen, C. Hierold and L. Wirtz, *Nano Lett.*, 2007, **7**, 238-242.

40 T. Abdiryim, X. Zhang and R. Jamal, *J. Appl. Polym. Sci.*, 2005, **96**, 1630-1634.

41 L. Zhang, Y. Long, Z. Chen and M. Wan, *Adv. Funct. Mater.*, 2004, **14**, 693-698.

42 C. K. Tan and D. J. Blackwood, *Sens. Actuators B*, 2000, **71**, 184-191.

43 C. Vallés, P. Jiménez, E. Muñoz, A. M. Benito and W. K. Maser, *J. Phys. Chem. C*, 2011, **115**, 10468-10474.

44 J. W. An, J. H. Liu, Y. C. Zhou, H. F. Zhao, Y. X. Ma, M. L. Li, M. Yu and S. M. Li, *J. Phys. Chem. C*, 2012, **116**, 19699-19708.

45 K. S. Subrahmanyam, S. R. C. Vivekchand, A. Govindaraj and C. N. R. Rao, *J. Mater. Chem.*, 2008, **18**, 1517-1523.

46 J. P. Pouget, M. E. Jozefowicz, A. J. Epstein, X. Tang and A. G. Macdiarmid, *Macromolecules*, 1991, **24**, 779-789.

47 H. K. Chaudhari and D. S. Kelkar, *Polym. Int.*, 1997, **42**, 380-384.

48 Y. P. Wu, B. Wang, Y. F. Ma, Y. Huang, N. Li, F. Zhang, and Y. S. Chen, *Nano Res.*, 2010, **3**, 661-669.

49 S. Liu, X. H. Liu, Z. P. Li, S. R. Yang and J. Q. Wang, *New J. Chem.*, 2011, **35**, 369-374.

50 Z.-D. Huang, R. Liang, B. Zhang, Y.-B. He and J.-K. Kim, *Compos. Sci. Technol.*, 2013, **88**, 126-133.

51 J. Zhang and X. S. Zhao, *J. Phys. Chem. C*, 2012, **116**, 5420-5426.